INTERNATIONAL ATOMIC ENERGY AGENCY
UNITED NATIONS EDUCATIONAL, SCIENTIFIC AND CULTURAL ORGANIZATION

INTERNATIONAL CENTRE FOR THEORETICAL PHYSICS
34100 TRIESTE (ITALY) - P.O.B. 586 - MIRAMARE - STRADA COSTIERA 11 - TELEPHONES: 224281/2/3/4/5/6
CABLE: CENTRATOM - TELEX 460392-1

SMR/100 - 28

WINTER COLLEGE ON LASERS, ATOMIC AND MOLECULAR PHYSICS

(24 January - 25 March 1983)

# High Resolution Atomic Spectroscopy in Discharges

a) Laser Magnetic Resonance
b) The Point Contact Diode at Laser Frequencies
c) Optogalvanic Spectroscopy

M. INGUSCIO
Istituto di Fisica
Università degli Studi
Piazza Torricelli, 2
56100 Pisa
Italy

extremely sensitive for recording rotational
Zeeman spectra in paramagnetic atoms and
molecules (EVENSON et al. 1980).
The sensitivity is close to the quantum
limit: MINIMUM DETECTABLE POWER at the
detector given by:

$$\Delta P(\min) = 4\,(P \cdot P_n)^{1/2} = 1.4\ 10^{-12}\ W \qquad (1)$$

TOTAL POWER $2.5\ 10^{-5}$ W — QUANTUM NOISE LIMIT ($4.7\ 10^{-21}$)

ACTUALLY IT IS DETERMINED by the Liquid Helium
cooled Ge bolometer (NEP $6.10^{-12}$ W – 1 Hz
band width) and by the laser source noise
(decreasing with increasing frequency of modulation
in a phase sensitive detection scheme).
A typical minimum detectable power is
$\sim 10^{-11}$ W for the stronger lines.
That corresponds to a minimum concentration
of $3 \times 10^{8}$ mol/cm$^{+3}$.

a source provided by the large amount
of stable (frequency reproducibility better
than $5 \times 10^{-7}$) of cw optically pumped
laser lines. The new spectrometer developed
at NBS is shown in the figure:

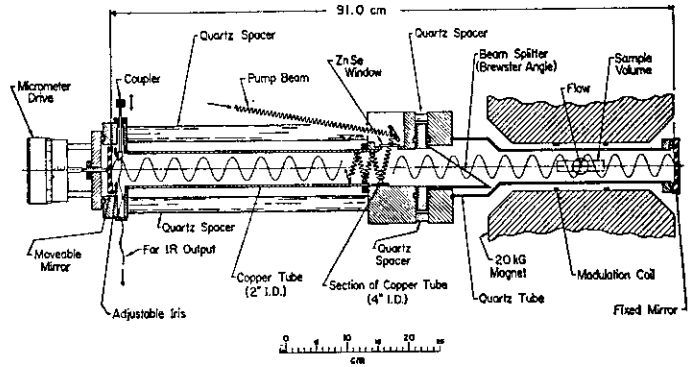


FIG. 1.—Laser magnetic resonance spectrometer, 40-1000 μm.

DIFFICULTIES FOR AN EXTENTION TO
ATOMS:

- SMALL PROBABILITY OF A "CLOSE" COINCIDENCE
  with a laser line (atoms posses much
  less eigenstates than a molecule)

- Allowed transitions are mostly magnetic dipole in nature (fine structure)

- Production of an enough number of atoms is even more difficult in case of refractory elements.

Interest for SILICON:

- Cosmic abundance $2.5 \times 10^{-5}$ (H): only H, He, O, N and C are more abundant
- Data only from optical spectroscopy
- No $g_J$ measurements
- Not yet astronomically detected at FIR wavelengths (important in cold interstellar clouds where optical spectra are not exited) – Ground state FINE STRUCTURE:

| | | |
|---|---|---|
| $^3P_J$ 2 —— | | |
| | 68.47 μm | $4 \cdot 10^{-5}$ sec$^{-1}$ (A) |
| 1 —— | | |
| | 129.7 μm | $8 \cdot 10^{-6}$ sec$^{-1}$ (A) |
| 0 —— | | |

The Zeeman scheme and the observed laser coincidences with the $J: 0 \to 1$ Si transition are shown in fig. 2.

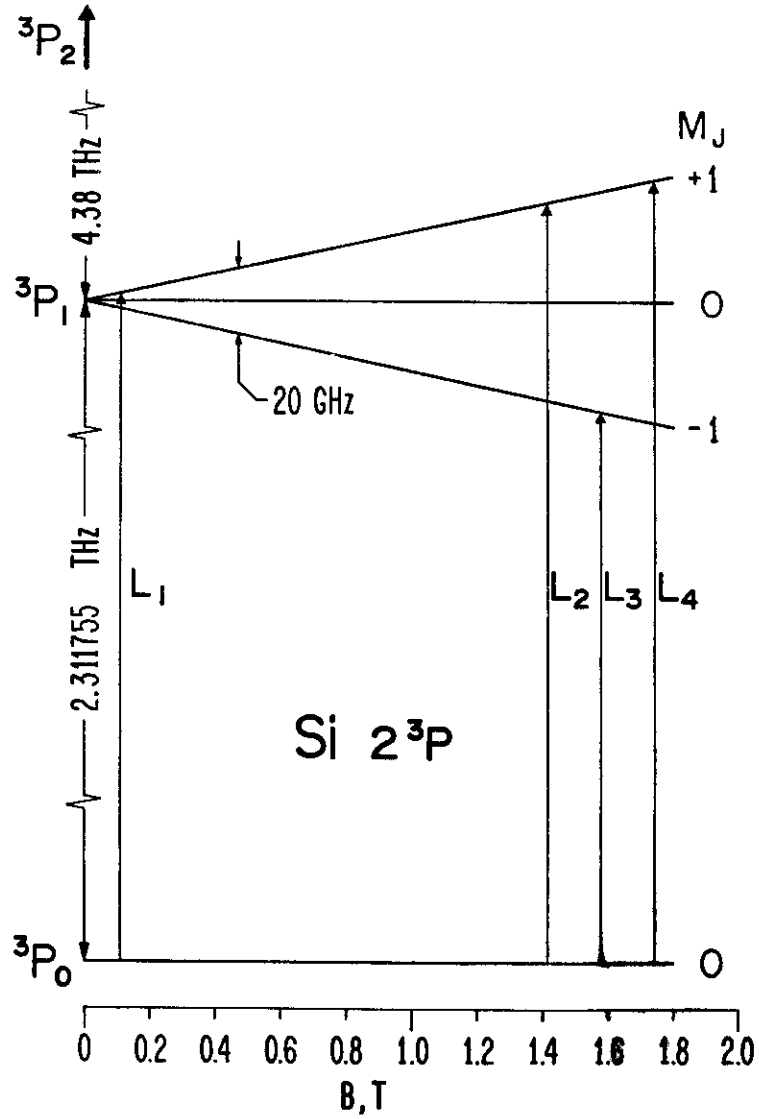


fig. 2

The atom was produced inside the FIR resonator in a reaction of atomic fluorine and $SiH_4$, and the atomic fluorine produced in a microwave discharge in a mixture of $F_2$ and He. In fig. 3 a typical LMR recording is shown (resonance with the 129.5 μm $CH_3OH$ laser line).

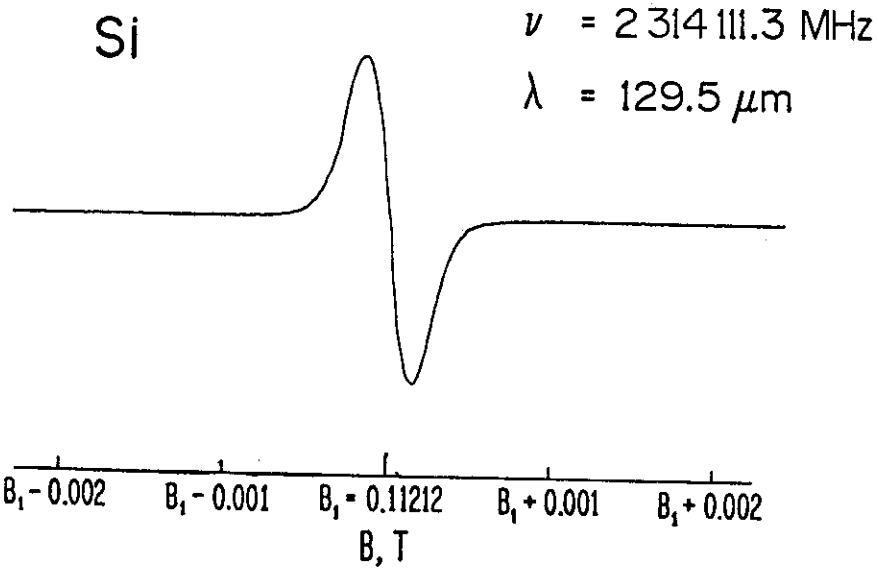


fig. 3

All the experimental data (laser frequencies, magnetic field values) are reported in the table:



TABLE 1.

EXPERIMENTAL LMR DATA FOR Si: $^3P_1 - {}^3P_0$ transition

| LASER LINE | B (Tesla) | TRANSITION $M''_J$ | TRANSITION $M'_J$ | $\lambda_L$ (μm) | LASING GAS | $\nu_L$ (MHz) |
|---|---|---|---|---|---|---|
| $L_1$ | 0.11212(1) | 0 | 1 | 129.5 | $CH_3OH$ | 2 314 111.3 |
| $L_2$ | 1.41212(10) | 0 | 1 | 128.3 | $CD_3OH$ | 2 341 508.9 |
| $L_3$ | 1.57900(10) | 0 | -1 | 131.6 | $CD_3OH$ | 2 278 703.0 |
| $L_4$ | 1.73964(17) | 0 | 1 | 127.7 | $^{13}CD_3OH$ | 2 348 438.4 |

The data are analyzed according to the usual 2nd order Zeeman equation (including the quadratic contribution (fig. 4):

$$\nu_L = \nu_0 + \mu_0 H\left[(g'_J - g''_J)M''_J \pm g'_J\right] + cH^2 \qquad (2)$$

$$\epsilon_1 = \mu_0^2/E_1 - E_0 \; ; \; \epsilon_2 = \mu_0^2/E_2 - E_1$$

$\nu_L$ is the laser frequency; $\nu_0$ the zero-field fine structure; $\mu_0$ is the Bohr magneton; c the

coefficient of the second order Zeeman shift ; $g_J$ the g factor of the state J - Primes and double primes refer to the upper and lower state of the transition.

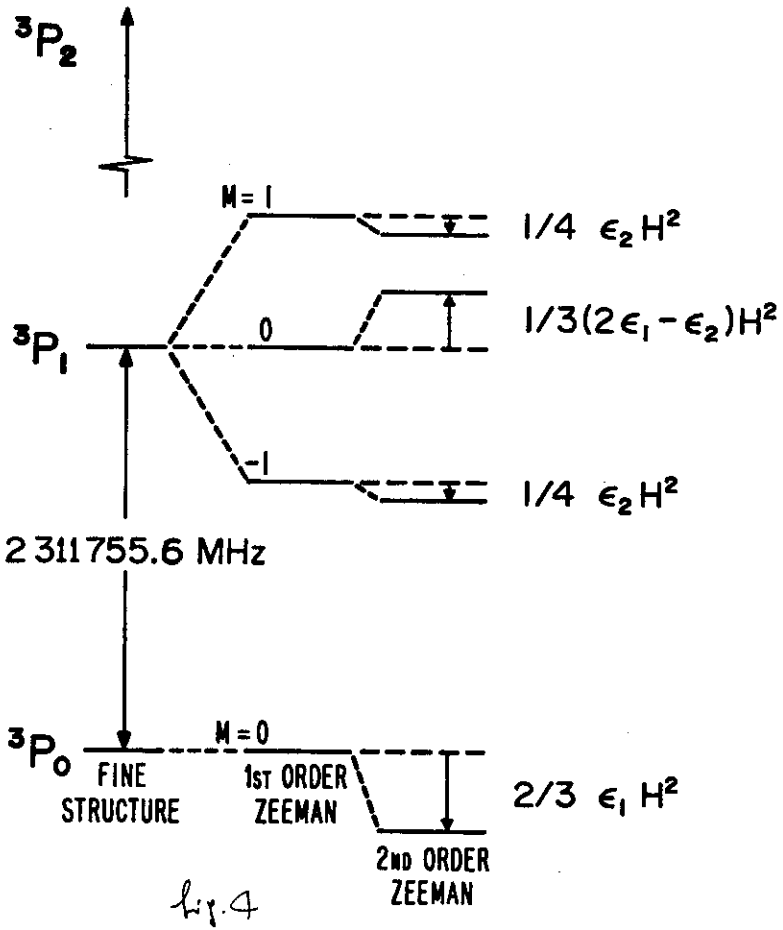


fig.4



From the experimental data precise values for $\Delta E$ and $g_J$ are obtained, which in Table 2 are compared with previous reported or computed values.

TABLE 2.

FINE STURCTURE SEPARATION $^3P_1 - {}^3P_0$ AND g FACTOR $^3P_1$ STATE:

| | PRESENT RESULT | PREVIOUS |
|---|---|---|
| $g_J$ : | 1.500 810 (40)[a] | 1.501 097[b] |
| $^3P_1 - {}^3P_0$ : | 2 311 755.6 (2) MHz. | 2 311.8 GHz[c] |

a. Calculated with $\mu_0$ = 1.39 9612 x $10^4$ MHz/TESLA, COHEN, E.R., AND TAYLOR, B.N. 1973, J. PHYS. CHEMS. REF. DATA, 2, 663.

b. *THEORETICAL VALUE, VESETH, L., PHYS. REV. 22, 803, (1980).

c. MOORE, CHARLOTTE E., SELECTED TABLES OF ATOMIC SPECTRA, NSRDS-NBS 3, SECTION 2, 1970.

FOR A RECENT REVIEW ON FIR LMR SPECTROSCOPY :

Evenson, K.M., R.J. Saykally, D.A. Jennings, R.F. Curl, J.M. Brown in: "Chemical and biochemical applications of lasers," C. Brodley Moore Ed. p. 95 Academic Press 1980.

## THE POINT CONTACT DIODE

The MIM (Metal Insulator Metal) point contact diode is the main element used in laser frequency synthesis. It is similar to the cat whisker diode used in the early radio receivers however it uses only metals and the natural oxide that forms on the nickel base as the insulator. The cat whisker is fabricated from a 10 to 25 μm diameter tungsten wire electrochemically sharpened to a tip radius of a few hundred Angstroms. The straight portion of the whisker from the tip to a right angle bend serves as antenna to concentrate the focused laser field at the tip where the non linear processes occurr at the nickel oxide layer.

The unknown frequency, $\nu_x$, is determined from the rf beat note when all the radiations



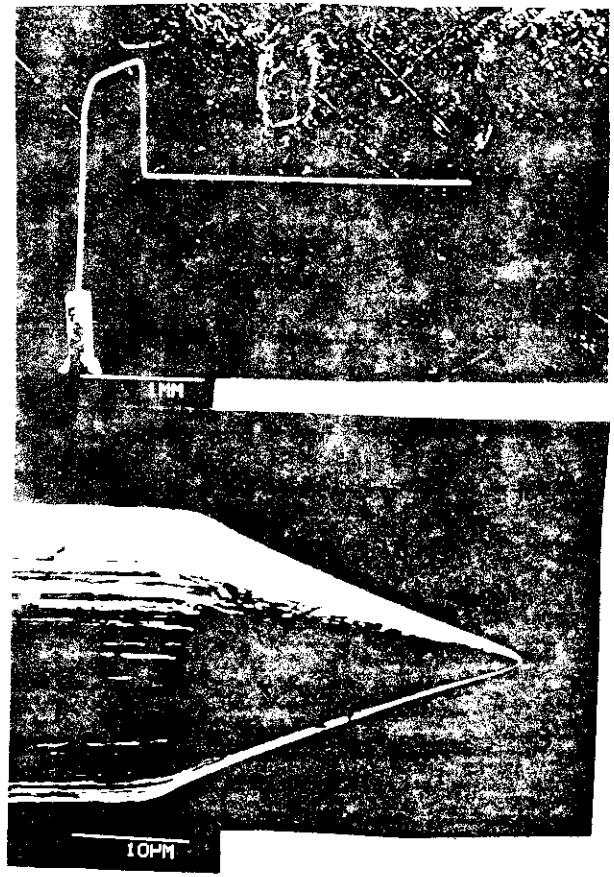


Fig 5

impinge on the diode. That is:

$$\nu_x = l\nu_l \pm m\nu_m \pm n\nu_n \pm \nu_b \qquad (3)$$

where $\nu_l$, $\nu_m$, and $\nu_n$ are known frequencies, $l$, $m$, and $n$ are the harmonics, and $\nu_b$ is the RF beat frequency. The MIM diode is

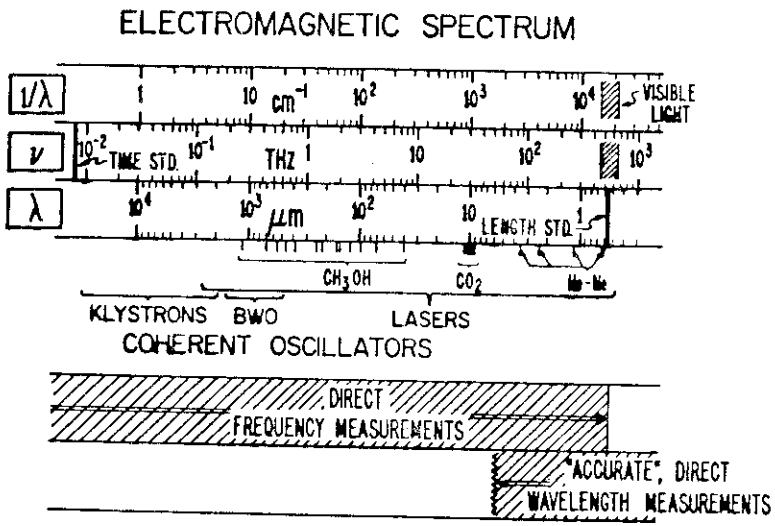


Figure 6. The electromagnetic spectrum showing oscillators, frequency and wavelength standards, and measurement regions. The extension of frequency measurements into the infrared has produced an overlap of the accurate ($< 4 \times 10^{-9}$) wavelength measurement region and the frequency measurement region for the first time. The frequency standard is the zero field hyperfine structure separation in the ground state of $^{133}Cs$ which is defined to be 9 192 631 770 Hz. The wavelength standard is the transition between the $2p_{10}$ and $5d_5$ levels of $^{86}Kr$ with the vacuum wavelength of this radiation defined to be 1/1 650 763.73 m.



the fastest broadband detector known: Its response time has been indicated with the generation of the 5th harmonic of $CO_2$ laser radiation (150 THz or $7 \times 10^{-15}$ sec) in the diode. It has been used from 100 MHz to the visible. The frequency measurement of visible light has produced an overlap of the accurate wavelength measurement region and the frequency measurement region for the first time (fig. 6). As a major result, the product of the measured frequency and the wavelength yields definitive values for the speed of light, c, nearly 100 times more accurate than the previously accepted value. (The value "recommended" by the CCDM is 299 792 458 m/sec with an uncertainty of about 4 parts in $10^9$). That is leading

to a new definition for the unit of length, the meter (presently 1,650,763.73 vacuum wavelengths of an orange-red spectral line of Krypton-86). The new proposal is "The meter is the length equal to the distance traveled in a time interval of 1/299 792 458 of a second".

New recent results on the diode are making the device even more stable and efficient hence allowing a systematic investigation of the sensitivity and the speed of response at different laser frequencies and mixing orders as a function of tip radius, coupling, and resistance.

Conical coupling

Instead of the smooth small angle antennae used in long wire coupling, larger angle



conical shapes were given to the end of the wire. In contrast with the conventional long-wire coupling, strong angular dependence

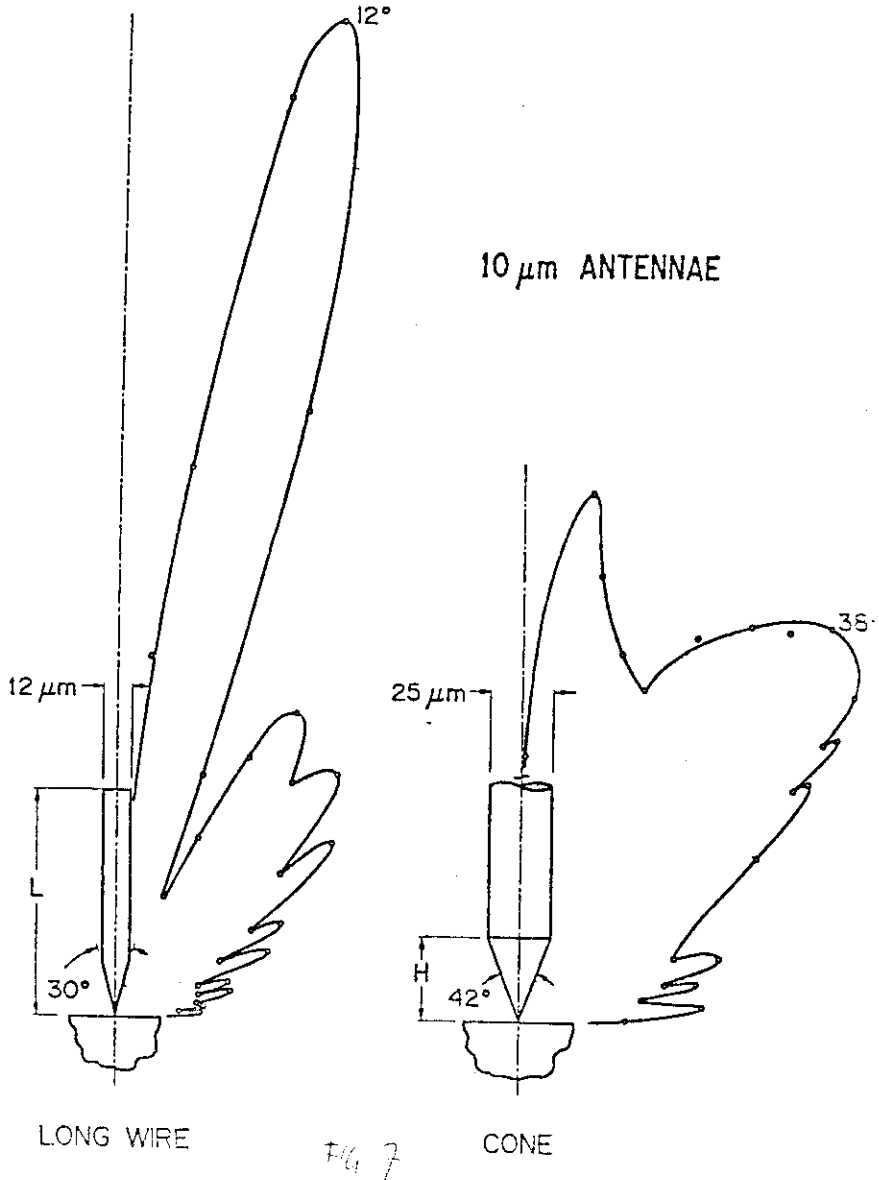


Fig 7

was absent for the conical coupling at 10 μm (FIG. 7). For these measurements a "plane wave" was approximated by focusing the radiation with a long focal length.

ADVANTAGES: COUPLING AT 45° independently of the WAVELENGTH ALLOWS EASY GEOMETRIES WHEN MORE THAN ONE LASER BEAM MUST BE SENT TO THE DIODE. The efficiency can be still improved using shorter focal length optics (increasing the coupling solid angle), while the long wire will only be degraded because the present focusing angle coincides with the major antenna lobe.

TIP RADIUS EFFECT–THIRD HARMONIC GENERATION

Most of the interest for point contact MIM diodes lies on their fairly high speed of response. To test that property as a function of the tip radius, the generation of third order signals was used. In fig. 8 is shown



the beat note (~30 db) obtained by mixing on the diode radiations from a 3.39 μm He-Ne laser, a 10 μm $CO_2$ laser, and from a klystron at 48 GHz. (The power was 30 mw from each laser)

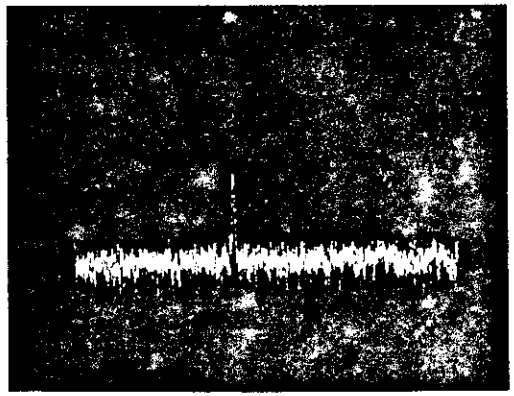

fig. 8

88 376 181.609 (He-Ne 3.39 μm) −
3 × 29 442 483.3197 ($CO_2$ 10 R 30) −
48 701.65 (Klystron) = 30 MHz

} FIFTH MIXING ORDER EXPERIMENT ($\ell+m+1$ in eqn. 3).

The signal to noise ratio of the heterodyne signal was measured as a function of the resistance for each diode, with tip radii from a few hundred angstroms to about 1 μm. Surprisingly the speed of response was not affected, as shown in fig. 9. That is important

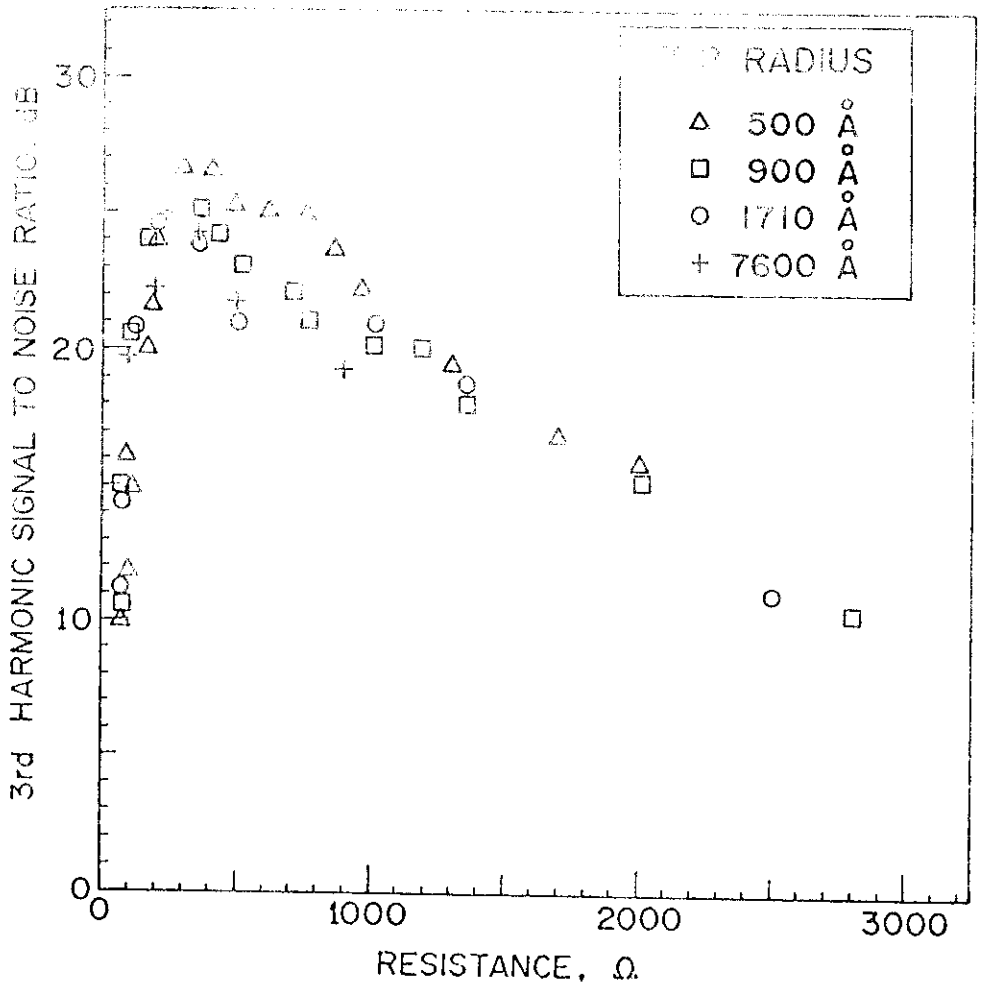


Fig 9

because all the theories up to now developed assume that the contact capacitance,



determined by the contact area, must be as low as possible to obtain a high frequency cut-off (for radii of some hundreds angstroms a frequency cut-off can be calculated of the order of 100THz and Radii of a few thousand angstroms should lead to a frequency cut-off two orders of magnitude lower i.e. in disagreement with the experimental results). Of course with the blunter tips the diode is much more stable and can be used for days at a time. Furthermore, the radius of the larger tips is greater than the spot size that can be made with lithography techniques: It may be possible to fabricate these devices with thin film technology into more or less permanent structures.

TWO DIFFERENT MECHANISMS

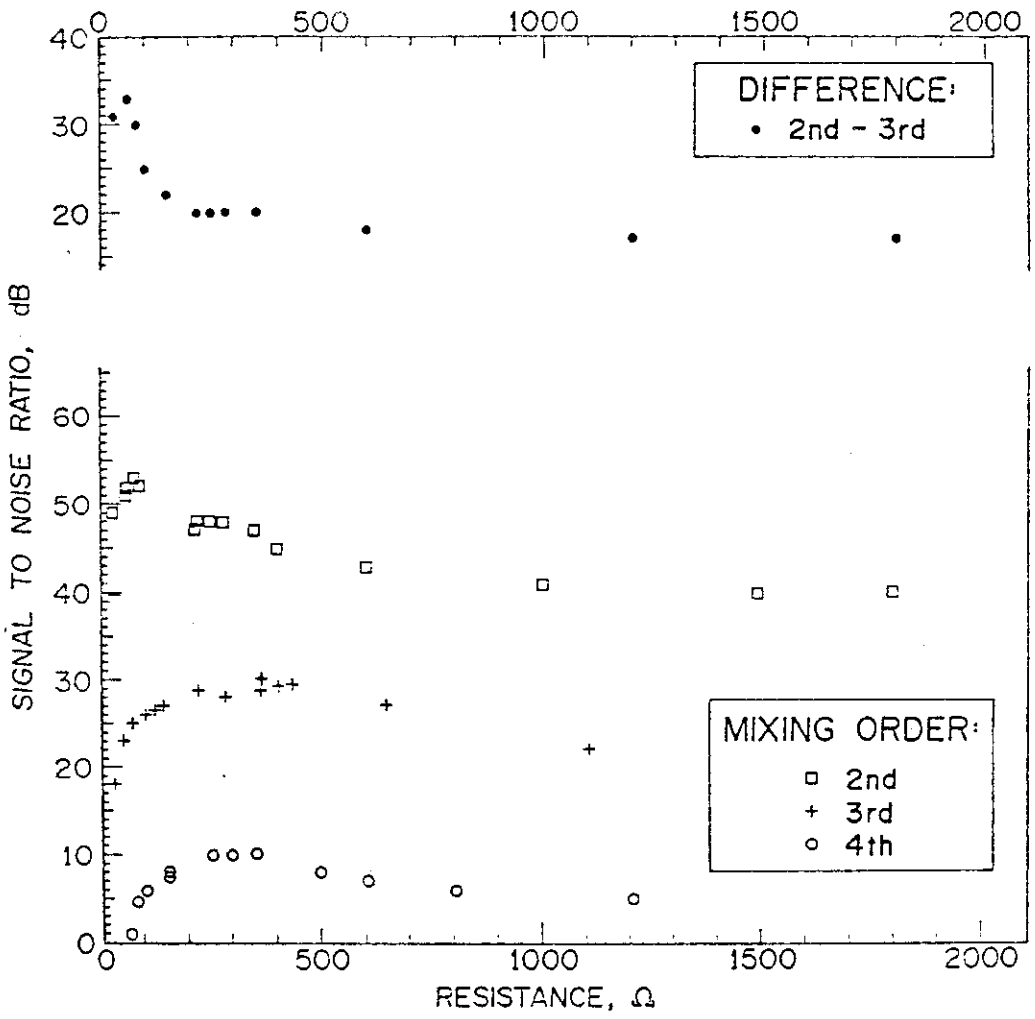


Fig 10

they are evidenced in the figure. (2nd order beating between two $CO_2$



lasers oscillating on the same line; 3rd between two $CO_2$ laser lines and a FIR laser; 4th between two $CO_2$, one FIR laser and microwave power). But the second mechanism is much slower (only present on the low-speed 2nd order measurement).

Conclusion: it is only the fast response mechanism (tunneling effect) responsible for the the operation as mixer all over the electromagnetic spectrum

Leferences:

K.M. Evenson, DA Jennings FK Petersen "The frequency measurement of visible light, J. Phys. 42 C 8-473 (1981)

M. Inguscio, K.M. Evenson, D.A. Jennings, F.R. Petersen "The Point Contact Diode at laser frequencies" App. Phys. lett. 1983

## LASER OPTOGALVANIC SPECTROSCOPY.

In LOG a tunable laser is used to probe the spectral characteristics of atomic or molecular species generated within an electrical discharge in a low pressure gas. Optogalvanic signals arise when the impedance of the discharge changes in response to the absorption of laser radiation (transition between levels with different ionization probability). For the many applications of the technique see the recent review by Webster and Rettner, Laser Focus, February 1983 and references therein.

Advantages for high resolution spectroscopy

- Saturation Subdoppler techniques typical of absorption spectroscopy (and in general limited to transitions starting from the ground or thermally populated states) can be applied to the whole emission spectrum of a lamp (including ionic or weak lines).

For instance in fig. 11 the optogalvanic doppler broadened curve of an excited transition in Neon is recorded together with two curves obtained in presence of counterpropagating laser beams hence exhibiting the lamb dips corresponding to the zero velocity atomic group.

The sensitivity and resolution of the technique



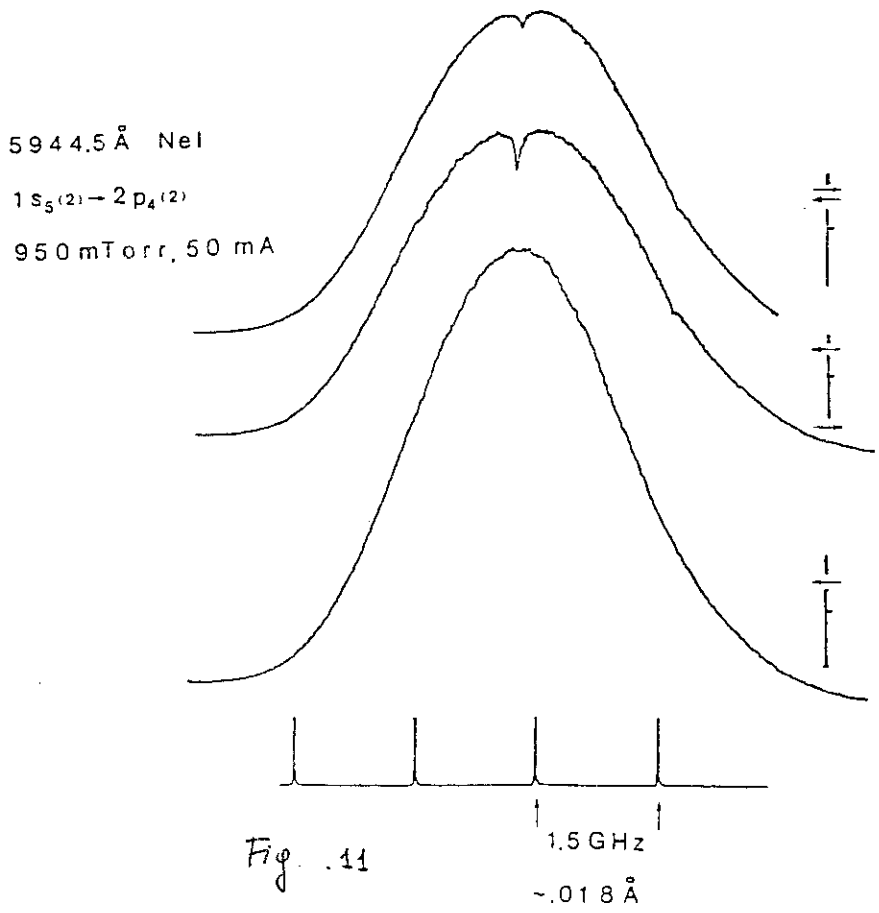


Fig. 11

can be improved using "intermodulated optogalvanic spectroscopy".

The metod consist in chopping the intensity of one of the counterpropagating laser beams at a frequency $f_1$ and the other at a frequency $f_2$. A $f_1$ signal

at a frequency $f_1 + f_2$ is recorded from a lock-in amplifier only when the two beams are interacting (and saturating) with the same group of atoms (zero axial velocity). A typical recording is shown in fig. 12, where, once the Doppler line broadening is eliminated, the Doppler-free intermodulated signals corresponding to the two $^{20}Ne$ 90.92% $^{22}Ne$ 8.823% isotopic components are well resolved. The broader

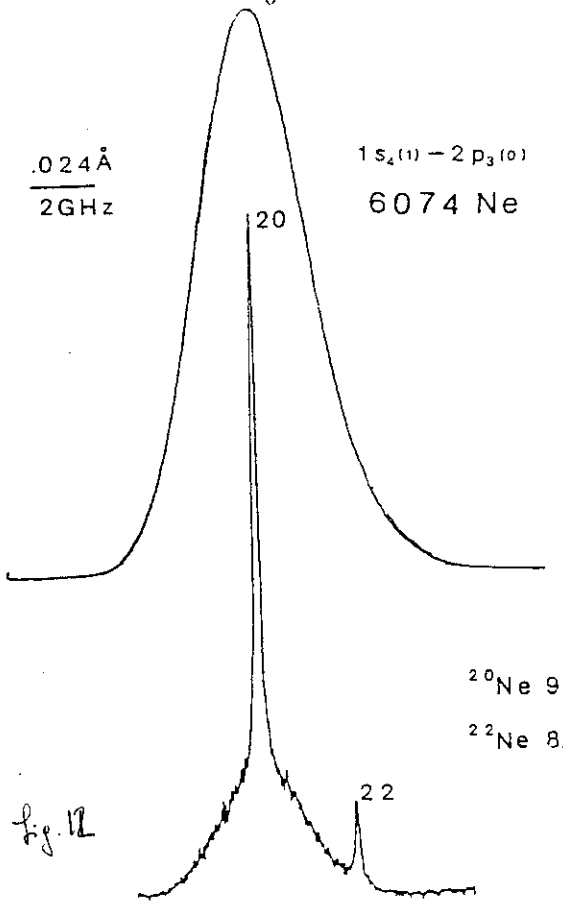


fig. 12



pedestal is caused by velocity changing collisions (i.e. an atom with non zero axial velocity can reverse its velocity component ~~with~~ along the laser beams direction so that it can interact with both the beams hence yelding a signal of $(f_1 + f_2)$).

The LOG technique can conveniently applied to non volatile elements sputtered into the gas substaining the discharge —

As an example in fig. 13 the isotopic and hyperfine structures of the Cu transition at 5782 Å are fully resolved (the experiment was done using a copper hollow cathode lamp, lower curve is recorded using the intermodulated scheme).

## LASER OPTOGALVANIC ZEEMAN SPECTROSCOPY

We have recently demonstrated (Opt. Commun. 43, 261, 1982) that a magnetic field can be conveniently applied on the discharge so that Zeeman effect can be investigated with LOG.

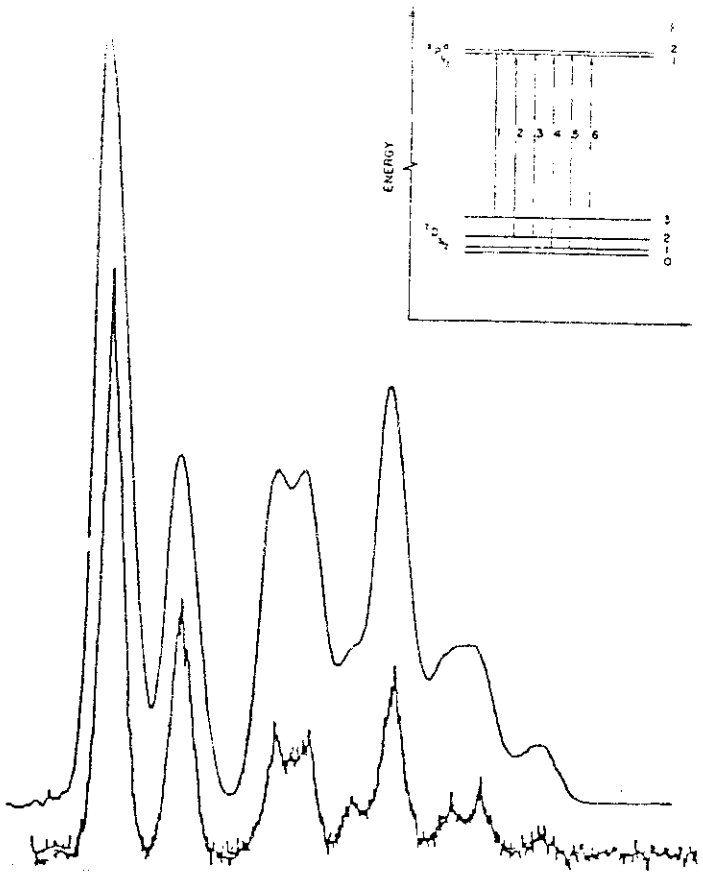


fig. 13

The apparatus is similar to the one for conventional intermodulated measurements, but a magnetic field, parallel to the discharge current, is applied using a couple of Helmholtz coils. The laser polarization (linear) is



orthogonal to the magnetic field so that transitions can be induced with both $\Delta M=+1$ and $\Delta M=-1$ selection rules.

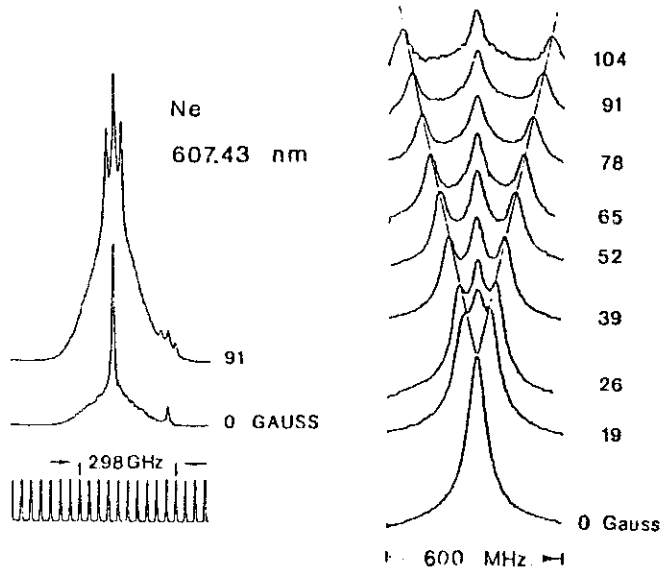


FIG 14

A typical example is shown in FIG 14 for a $J: 0 \rightarrow 1$ transition. The good signal to noise ratio allows the resolution of the Zeeman structure for both the isotopic components. Thanks to the resolution of the technique the effect can be investigated from very low values of the magnetic fields. The peaks at the center of the recordings correspond to the "cross-over" signal, typical of saturation spectroscopy of transitions sharing a common level. Resolution and signal to noise are not affected by the rather high currents (~100mA)

necessary for investigating non volatile elements. A result for the $^3P_0 \rightarrow {}^3S_1$ transition in Calcium is reported in FIG. 15. The arrows refer to the theoretical $\Delta M=+1$ and $\Delta M=-1$ components, while the central peak is again a crossover signal.

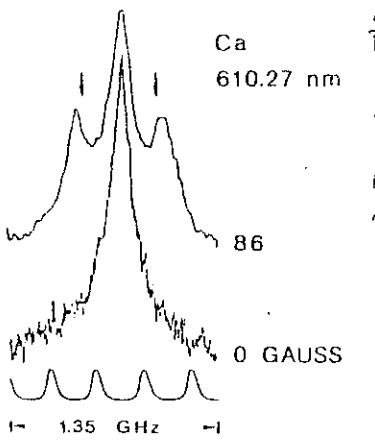


FIG 15

LOG spectroscopy, like other techniques (optoacoustic or Laser induced fluorescence) based on the detection of signals directly related to the absorbed energy in the interaction radiation – atomic system is well suited for the investigation of even small effects which should be masked in a transmitted radiation detection scheme. One of these, related to the saturation in the interaction laser – atomic transition, is the

NON LINEAR HANLE EFFECT

It is caused by the different saturation of the M components of an inhomogeneous line



in presence or not of an external field which removes the degeneration.

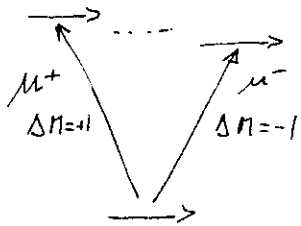


Fig. 16

Differently from the conventional linear case, the effect causes a change in the absorption of the saturating laser radiation. (A peculiarity of this technique is that the resolution of the components leads to an increase of the absorption, and not to a decrease typical of all other techniques). As is well known in presence of saturation the absorption coefficient of a doppler broadened line can be written:

$$I(\omega) = \frac{\alpha |\mu|^2}{(1+I/I_s)^{1/2}} \exp -\left[(\omega-\omega_0)/\Delta_D\right]^2 \qquad (4)$$

where $\mu$ is the matrix element of the transition, $\omega_0$ its center frequency, $\Delta_D$ the Doppler linewidth, $I/I_s = S$ the saturation parameter. When the degeneration of the M sublevels is removed, each transition saturates independently. As an example for a $0 \rightarrow 1$ transition (Fig. 16) and a static field polarized orthogonal to the static field ($\Delta M = \pm 1$) the absorption is given by eq. 4 when the static field intensity is negligible and by

$$I^F = \frac{\alpha|\mu^+|^2}{\left(1+\frac{I^+}{I_s}\right)^{1/2}} e^{-\frac{(\omega-\omega_0^+)^2}{\Delta_D}} + \frac{\alpha|\mu^-|^2}{\left(1+\frac{I^-}{I_s}\right)} e^{-\left(\frac{\omega-\omega_0^-}{\Delta_D}\right)^2} \quad (5)$$

when the degeneracy of the levels is removed.
Since $|\mu|^2 = |\mu_+|^2 + |\mu_-|^2$, one obtains an increase of the absorption given by

$$I^F/I = \left(\frac{1+2S}{1+S}\right)^{1/2} \quad (6)$$

A prediction of the theory is that the effect should be observed at any setting of the laser frequency, within the Doppler profile, scaled by a gaussian factor —
An experimental demonstration is

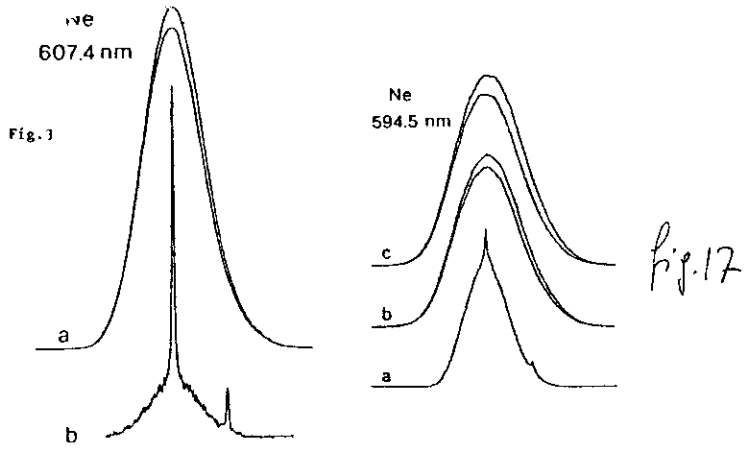


Fig. 3

fig. 17



in fig. 17 when the LOG signals on two different transitions of Ne is recorded in presence and absence of a magnetic field. Note that the detected enhancement is asymmetric due to the presence of the two isotopes, hence of two overlapping Doppler curves.

On the right side of the figure the rotating laser intensity is changed (22 mW in b and 65 mW in c) and correspondently the relative enhancement is 8% in b and 13% in c.

A quantitative analysis can be performed measuring the enhancement as a function of the applied magnetic field. Since Zeeman fields also tune the

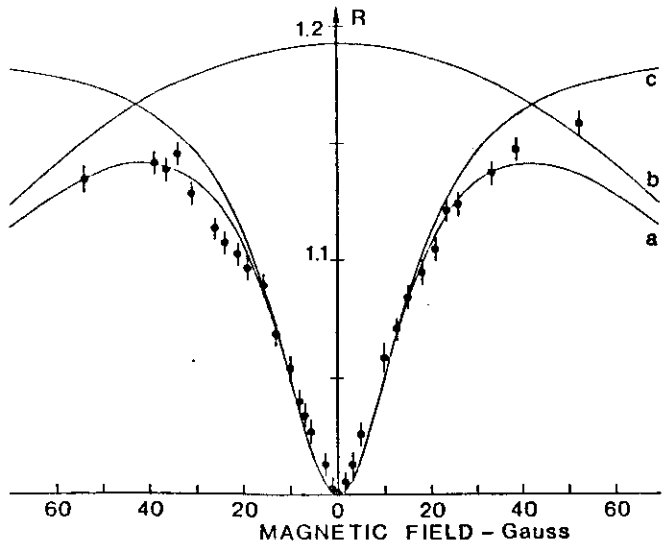


fig. 18

transition along the Doppler broadened profile, the NLHE curve (one negative Lorentzian) is superimposed to a gaussian shaped decrease. The experimental data of fig. 18 refer to the Ca transition at 6102 Å and illustrate the general features of the technique.

Curve b) refers to the fit using a Lorentzian plus a Gaussian, while the two curves as resulting from the fit are separately displayed in c) and a). From the amplitude of the Lorentzian $I/I_s = 2.21$ is extracted. The value is used to evaluate the contribution of saturation to homogeneous broadening and the collisional linewidth is obtained.

For a generalization to any J and $\Delta J$ and further details see:

M. Inguscio, A. Moretti, F. Strumia Appl. Phys. B28, 88 (1982) and references therein.